sciendo

DOI 10.2478/ama-2021-0025

acta mechanica et automatica, vol.15 no.4 (2021)

# APPLICATION OF MAGNETIC AND ULTRASONIC METHODS FOR DETERMINING PARAMETERS OF FERROMAGNETIC COMPONENTS IN IRON ORE SLURRY FLOWS

**Vladimir MORKUN[*], Natalia MORKUN[*], Vitaliy TRON[*], Olga PORKUIAN[**], Oleksandra SERDIUK[*], Tetiana SULYMA[***]**

[*]Automation, Computer Science and Technologies Department, Kryvyi Rih National University, Vitalii Matusevich Street, 11, Kryvyi Rih, Ukraine
[**]Volodymyr Dahl East Ukrainian National University, Central Pr. 59-a, Severodonetsk, Ukraine
[***]Kryvyi Rih National University, Vitalii Matusevich Street, 11, Kryvyi Rih, Ukraine

morkunv@gmail.com, nmorkun@gmail.com, vtron@ukr.net, porkuian@i.ua, o.serdiuk@i.ua, sts.1811@ukr.net

*received 13 August 2019, revised 19 July 2021, accepted 23 July 2021*

**Abstract:** The article considers the method for controlling the ferromagnetic component content in slurry flow by ultrasonic and magnetic measurements. One of the basic factors determining the efficiency of magnetic separators at iron ore concentration plants is the quality of distribution of the ground ore into the product containing the ferromagnetic component and the waste rock. Due to the fact that in most cases, magnetic separators extract minerals with strongly magnetic properties, it is essential to find the magnetic component content in the input ore and products of its distribution in order to improve control over the technological process. Currently, low accuracy and reliability make existing means of operative control over the ferromagnetic component content in the slurry flow inefficient. Density of slurry is one of the primary disturbing factors affecting the accuracy of measurements, and this fact determines the necessity of measuring this parameter while controlling the ferromagnetic component content. Combined methods of measurements are a promising trend in designing sensors of useful component content in the slurry flow. The article describes the method for controlling the ferromagnetic component content in slurry flow by ultrasonic and magnetic measurements.

**Key words:** ferromagnetic component, ultrasound, slurry, ore, lamb waves

## 1. INTRODUCTION

The efficiency of controlling processes in iron ore concentration is mostly conditioned by the frequency and accuracy of the data entry of the process parameters (Kupin, 2014; Hauptmann et al., 2002; Stupnik et al., 2015; Semerikov and Slovak, 2011; Modlo et al., 2019).

Ultrasonic waves are applied for controlling the characteristics of technological media (Rzhevsky and Yamshchikov, 1968; Seip et al., 1996; Brazhnikov, 1975; Bond et al., 2003) as they enable signals from any point of the propagation surface and have relatively larger concentration of energy in a wave due to their smaller layer of localisation. The walls of technological vessels and industrial aggregates in iron ore concentration are mostly made of metal sheets to conduct ultrasonic control of parameters of contacting media, thus influencing the efficiency of Lamb waves. These waves are less susceptible to the impacts of disturbing factors than other types of ultrasonic waves. It should be noted that Lamb waves are also less susceptible to the condition of the surface of wave propagation and the action of gas bubbles in the studied medium. In other words, application of Lamb waves ensures the set error in measuring parameters of the ferromagnetic component of the iron ore slurry at the concentration plant (Zhang et al., 2020; Xu and Hu, 2017).

Thus, investigation into Lamb waves propagating on the plate in contact with the iron ore slurry with the purpose of determining the parameters of the ferromagnetic component of the flow is quite promising and topical (Ni and Chen, 2018; Meng and Yan, 2019).

## 2. LITERATURE ANALYSIS AND PROBLEM

### 2.1. Statement

Ways of increasing the efficiency of ore material concentration are considered in previous papers (Golik et al., 2015a; 2015b; Liu et al., 2020; Ma et al., 2019; Eremenko et al., 2019). It is worth emphasising that obtaining on-line data on technological process and iron ore characteristics is a problem in technological flows in particular (Lolaev et al., 2018). For exerting control over concentration processes and characteristics of the ore slurry, Morkun et al. (2015a; 2015b) suggest using controlled ultrasonic waves.

Regularities of propagation of ultrasonic waves in liquid under the cavitation mode have been studied previously (Louisnard, 2012a; Yuan et al., 2018; Wan et al., 2020; Zhao et al., 2019). Computing methods allow calculation of the energy dispersed by bubbles. There is a direct dependency of the energy lost by bubbles and attenuation of ultrasonic oscillations, which results in progressive waves. The above-described results (Louisnard, 2012b) enable the calculation of the Bjerknes force and prediction of bubble structures formed under the action of progressive waves.

Multimode Lamb waves have been used as a means of non-

destructive control by Ryden et al. (2003). By measuring the various modes in experimental curves of dispersion of Lamb waves and comparing them with theoretical curves, some physical parameters of the medium under study are obtained. It is observed that the dispersion curves of Lamb waves depend only on the parameters of the plate, while their frequency and phase velocity can be standardised according to the velocity of shear waves and the thickness of the medium's layer under study.

As noted previously (Debarnot et al., 2006), the advantage of Lamb waves in the context of nondestructive control of various ultrasonic waves is that one is able to check a larger area by using a minimum number of receivers. As Lamb waves are dispersive, a sinusoidal signal of emission is recommended. Lamb waves were simulated by applying the ATILA software.

Previous investigations (Lee and Staszewski, 2009) also indicate that Lamb waves are the most widely used ultrasonic waves applied for controlling various media. Yet, theoretical analysis of controlled wave propagation is a complicated task to perform. The method for simulating local interaction in wave propagation in metallic structures is considered. It is worth noting that application of the suggested method is complicated by at least two coexisting highly dispersive modes at any set frequency.

The method for controlling the parameters of liquid media by ultrasonic Lamb waves is presented by Subhash and Krishnan (2011). It is shown that changes in wave characteristics can be used as a function depending on the liquid level. As indicated, it is necessary to conduct some additional investigations to determine the optimal conditions of the measured parameters of the liquid medium by applying Lamb waves.

It follows from other studies (Viktorov, 1966; 1975) that availability of the magnetic field causes auxiliary attenuation and velocity dispersion of the volume of ultrasonic waves propagating in the studied medium.

Analysis of scientific sources (Fukumoto et al., 2019; Eskandari and Hasanzadeh, 2021; Parekh et al., 2015; Porkuian et al., 2020; Parekh and Upadhyay, 2017) indicates that in most cases, certain wave types have been used to develop methods of ultrasonic control of the characteristics of heterogeneous media. To solve the set tasks, the choice of a particular wave type requires consideration of a number of strict requirements and limitations imposed on both characteristics of the propagation surface and properties of the controlled medium. Lamb waves can be considered promising for determining the parameters of the ferromagnetic component of the iron ore slurry flow. At the same time, the problem of assessing the scale of impact of the ferromagnetic properties of the slurry's solid phase on the results of the measured parameters of these propagating waves remains unsolved.

## 3. RESEARCH AIM AND TASKS

The research aims at elaborating the method of controlling the ferromagnetic component content in the slurry flow by studying the impact of the ferromagnetic properties of the slurry's solid phase on the results of ultrasonic and magnetic measurements.

To achieve the set goal, it is necessary to solve the following tasks:

- Study the dependencies of the relative volume magnetic susceptibility of an aggregate on the volume concentration of magnetite inclusions;
- Study the dependency of the magnetic susceptibility of the slurry on the volume concentration of magnetite;
- Develop a scheme of measuring the ferromagnetic component in the iron ore slurry flow by ultrasonic and magnetic methods.

## 4. MATERIALS AND RESEARCH METHODS

Let us consider the method of measuring the ferromagnetic component in the iron ore slurry by applying Lamb waves to determine the concentration of the slurry solid phase and assess its magnetic susceptibility.

The method of assessing the intensity of Lamb waves is used to define the solid component content in the iron ore slurry.

If the plate along which the Lamb waves are propagating contacts the liquid and the sound velocity in the liquid $C_{liq}$ is smaller than the velocity of the Lamb wave in the plate $C$, the Lamb wave will attenuate, emitting energy into the liquid. The attenuation factor of the Lamb wave per unit length is determined by the following expression (Viktorov, 1966; 1975; Morkun et al., 2014; Morkun et al., 2015c):

$$k_2 = -i\frac{\rho_{liq}}{\rho}k_1 \cdot A_{s,a}, \tag{1}$$

where $\rho_{liq}$ is the density of the liquid contacting the plate surface; and $\rho$ is the density of the plate material.

$$A_{s,a} = -\frac{ik_t^4 th(S_{s,a}\cdot d)}{8k_{s,a}^2 \cdot S_{s,a}\sqrt{k_c^2 - k_{s,a}^2}}\left[1 + \frac{k_{s,a}^2}{2S_{s,a}^2} + \frac{k_{s,a}^2}{2q_{s,a}^2} - \right.$$
$$- \frac{4k_{s,a}^2}{k_{s,a}^2 + S_{s,a}^2} + \frac{k_{s,a}^2 \cdot d}{2S_{s,a}}(thS_{s,a}d - cthS_{s,a}d) -$$
$$\left. - \frac{k_{s,a}^2 \cdot d}{2q_{s,a}}(thq_{sa}d - cthq_{s,a}d)\right]^{-1}, \tag{2}$$

where $k_{s,a}$ is the wave number of symmetric and antisymmetric Lamb waves; $d$ is the plate thickness; $k_c$ is the wave number of ultrasound in the fluid;

$$q_{s,a} = \sqrt{k_{s,a}^2 - k_l^2}; \tag{3}$$

$$S_{s,a} = \sqrt{k_{s,a}^2 - k_t^2}; \tag{4}$$

$k_l$ and $k_t$ are wave numbers of the longitudinal and transversal waves of the plate material.

It should be noted that the attenuation factor of Lamb waves steadily rises while $\rho_{ж}\cdot\rho^{-1}$ increases. It means that $k_2$ can be presented as

$$k_2 = \frac{\rho_c}{\rho}C_v, \tag{5}$$

where $C_v$ is the value practically independent of liquid density and a function of the wave numbers of Lamb, longitudinal and transversal waves of the plate material.

As the gas phase of the slurry has almost no influence on its density, gas bubbles will not affect the attenuation of Lamb waves. In this case, the slurry density $\rho_{liq}$ will be determined by the volume fraction of the solid phase particles in the slurry $W$, their average density $\rho_{sol}$ and the liquid density $\rho_w$:

$$\rho_{liq} = (1 - W)\rho_w + W\rho_{sol}. \tag{6}$$

Therefore, the attenuation factor $k_2$ can be presented as

$$k_2 = \left[(1-W)\frac{\rho_w}{\rho} + W\frac{\rho_{sol}}{\rho}\right] C_v. \quad (7)$$

Thus, the intensity of Lamb waves at distance $l$ from the wave source can be determined by the following formula:

$$I_{l,v} = I_{0,v} \cdot exp\{-k_2 l\} = \\ = I_{0,v}\, exp\left\{-[(1-W)\frac{\rho_w}{\rho} + W\frac{\rho_{sol}}{\rho}]C_v l\right\}. \quad (8)$$

If in Eq. (8), $W = 0$, we obtain the expression that conditions the intensity of Lamb waves when the plate contacts pure water:

$$I^*_{l,v} = I_{0,v}\, exp\left\{-\frac{\rho_w}{\rho} C_v l\right\}. \quad (9)$$

It is easy to demonstrate that considering Eq. (9), Eq. (8) can be presented as follows:

$$I_{l,v} = I^*_{l,v}\, exp\left\{-W\frac{[\rho_{sol}-\rho_w]}{\rho} C_v l\right\}. \quad (10)$$

As seen from Eq. (10), the signal

$$S = ln\left(\frac{I^*_{l,v}}{I_{l,v}}\right) = W\frac{[\rho_{sol}-\rho_w]C_v l}{\rho}, \quad (11)$$

is proportional to the volume fraction of the solid in the slurry $W$ and does not depend on gas bubbles' availability.

Let us analyse the basic factors determining magnetic susceptibility of the iron ore slurry.

As is known, magnetic susceptibility is determined by the following relation (Bogdanov, 1983):

$$\mu_r = 1 + \chi\rho, \quad (13)$$

where $\chi$ is volume magnetic susceptibility.

According to their magnetic properties, ore minerals are divided into strongly and weakly magnetic. Rock-forming minerals are usually non-magnetic.

Magnetite ($FeO{\cdot}Fe_2O_3$) is a basic strongly magnetic iron-bearing mineral. According to Karmazin and Karmazin (1978), it is characterised by the following parameters: Curie point $\theta$ = 578° C; saturation magnetisation $J_s$ = 451–454 kA/m; coercive force $H_c$ = 1.6 kA/m; initial specific magnetic susceptibility $\chi$ = (0.18−1.28) × $10^{-2}$ $m^3$/kg. Magnetic saturation of magnetite starts with magnetisation in the field of 320 kA/m.

Tab. 1 presents the data on the magnetic properties of weakly magnetic iron-bearing minerals. One of the basic peculiarities of strongly magnetic substances is the dependency of their magnetic flux density or magnetisation on the field intensity. Fig. 1 depicts the dependency of specific magnetic susceptibility of magnetite on the magnetic field intensity.

The magnetic properties of magnetite are also dependent on the particle size. When particles become smaller, the coercive force rises, while the specific magnetic susceptibility falls (Karmazin and Karmazin, 1978). Specific magnetic susceptibility is determined using the expression

$$\chi_0 = \frac{\chi}{1+N\rho_{sol}\chi}, \quad (14)$$

where $\rho_{sol}$ is the density of solid particles; $N$ is the demagnetisation factor established to be equal to 0.16 for magnetite (Karmazin and Karmazin, 1978).

Fig. 2 shows the dependency of magnetic susceptibility $\chi$ of pure magnetite on particle size $r$. Specific magnetic susceptibility of the magnetite aggregate with weakly magnetic or non-magnetic minerals depends only on magnetite content. It is explained by the fact that the specific magnetic susceptibility even of martite, with relatively high specific susceptibility of $\chi \approx 9 \times 10^{-6}$, is 100-fold lower than that of magnetite, and that of other weakly magnetic minerals is even several-fold lower.

**Tab. 1.** Magnetic properties of weakly magnetic iron-bearing minerals

| Minerals | Chemical formula | Fe content in pure mineral, % | Specific magnetic susceptibility, $\chi$ $10^{-8}$ $m^3$/kg |
|---|---|---|---|
| Magnetite | $Fe_3O_4$ | 72.4 | < ~1,20,000 |
| Martite | $Fe_2O_3$ | 70.0 | < ~880 |
| Hematite | $Fe_2O_3$ | 70.0 | 80–220 |
| Siderite | $FeCO_3$ | 48.2 | ~75 |
| Brown hematite | $nFe_2O_3{\cdot}mH_2O$ | up to 60.0 | 40–90 |
| Goethite | $FeO{\cdot}OH$ | 62.9 | ~32 |

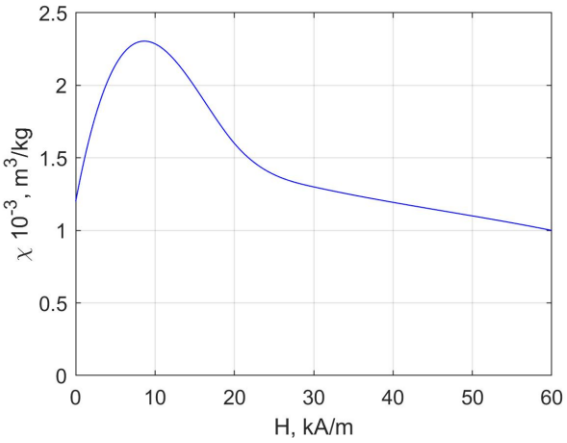


**Fig. 1.** Dependencies of specific magnetic susceptibility on the magnetic field intensity

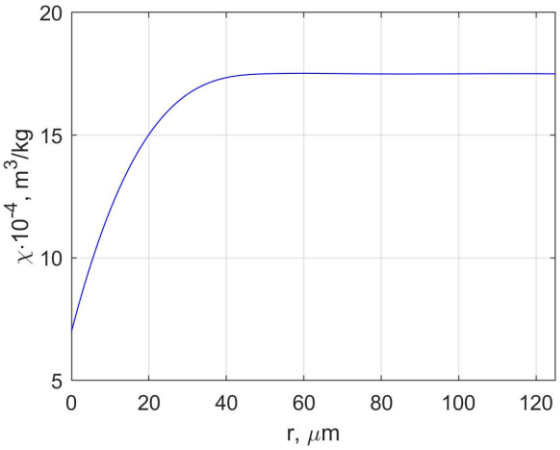


**Fig. 2.** Dependency of specific magnetic susceptibility χ on magnetite particle size

Fig. 3 provides the dependency of the relative volume magnetic susceptibility $\lambda$ of the aggregate – as a ratio of the volume susceptibility of the aggregate $\chi_{aver}$ to the volume susceptibility of pure magnetite $\chi$ – on the volume concentration of magnetite $C_m$ under three variants of non-magnetic inclusions. In the

first variant, inclusions are shaped as ellipsoids the long axis of which is parallel to the field intensity (Fig. 4); in the second variant, they are shaped as balls, and in the third variant, as ellipsoids the long axis of which is perpendicular to the field (Bogdanov, 1983; Karmazin and Karmazin, 1978; Weinberg, 1966; Derkach, 1966).

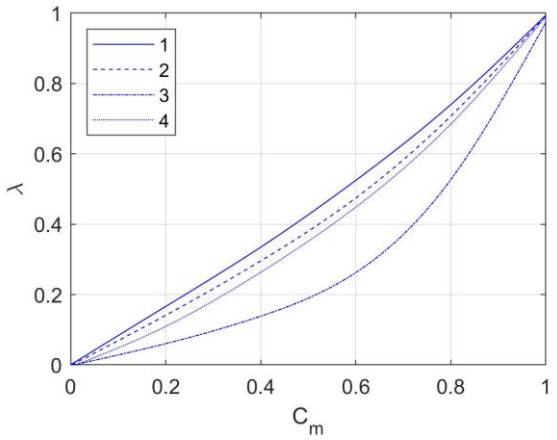


**Fig. 3.** Dependency of relative volume magnetic susceptibility of the aggregate on the volume concentration of magnetite inclusions: 1 – inclusions shaped as ellipsoids; 2 – inclusions shaped as balls; 3 – inclusions shaped as ellipsoids the long axis of which is perpendicular to the field; 4 – averaged characteristic

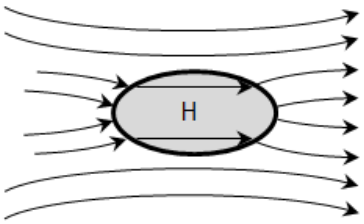


**Fig. 4.** Scheme of magnetisation in a magnetic field of a ferromagnetic ellipsoid the long axis of which is parallel to the field

It is evident that as the shape of non-magnetic inclusions and location of their long axis in relation to the field in the aggregate can vary, for practical purposes, only averaged values can be used in determining the value of $\lambda$.

## 5. INVESTIGATION RESULTS

For practical purposes, while determining the relative volume magnetic susceptibility of the aggregate under the field intensity of ≈50 kA/m, if ore formations are extracted from magnetite, the following expression is most often used (Karmazin and Karmazin, 1978):

$$\lambda = \frac{\chi_{spl}}{\chi_0} = 10^{-4}\alpha^2, \quad (15)$$

where $\chi_{spl}$ is the volume magnetic susceptibility of the aggregate; $\chi_0$ is the volume magnetic susceptibility of particles of pure magnetite, and $\alpha$ is the magnetite content in the aggregate.

When passing from volume magnetic susceptibility to the specific one, it should be taken into account that the density of the aggregate rises when the magnetite content increases. For example, if the slurry solid phase consists of magnetite of ≈5 × $10^3$ kg/m$^3$ density and rock-forming minerals, such as quartz and silicate, of ≈2.8 × $10^3$ kg/m$^3$ density, the magnetic susceptibility of the aggregate is

$$\chi'_{spl} = \frac{\chi_{spl}}{\rho_{spl}} \approx \frac{1.13\cdot 10^{-5}\alpha^2}{127+\alpha}, \quad (16)$$

where $\rho_{spl}$ is the density of the aggregate.

Fig. 5 shows the dependency of the relative specific magnetic susceptibility $K$ on the magnetite content in the aggregate $\alpha$.

As the specific susceptibility of inclusions of weakly magnetic and non-magnetic minerals does not depend on the field intensity and particle shape, their magnetic susceptibility is determined by the following expression:

$$\chi_{spl} = \sum_{i=1}^{\omega} \alpha_{im}\,\chi_{im}, \quad (17)$$

where $\alpha_{im}$ is the content of the weakly magnetic or non-magnetic *i*-th mineral in the aggregate; $\chi_{im}$ is specific magnetic susceptibility of the weakly magnetic or nonmagnetic *i*-th mineral.

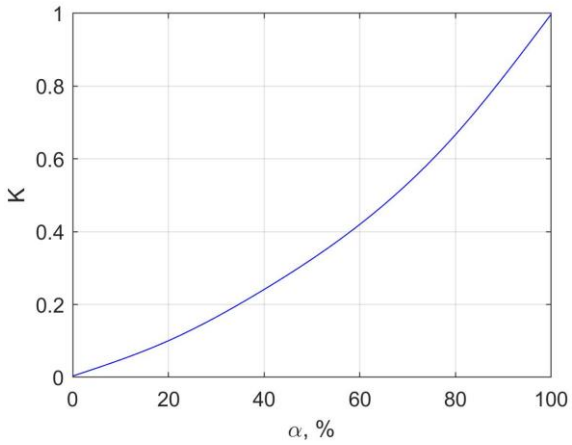


**Fig. 5.** Dependencies of the relative specific magnetic susceptibility $K$ on the magnetite content in the aggregate $\alpha$

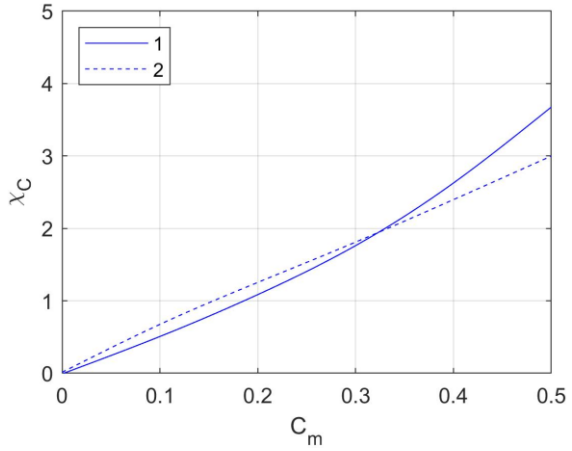


**Fig. 6.** Dependency of the volume magnetic susceptibility on the volume concentration of magnitite: 1 – theoretical; 2 – experimental

Magnetic susceptibility of the controlled material is dependent not only on the volume concentration of magnetite but also on the medium in which its particles occur. Magnetic susceptibility of the iron ore slurry is almost directly proportional to the magnetite

concentration (Bogdanov, 1983; Karmazin and Karmazin, 1978; Weinberg, 1966; Derkach, 1966).

Fig. 6 provides the experimental dependency of slurry susceptibility on volume concentration of magnetite (slurry density is 1,350 g/cm$^3$, the content of 74 particles makes 75%). Similar dependency is obtained via computation. Differences between the theoretical and experimental results with large magnetite concentrations can be apparently explained by the interaction of particles within the slurry that makes their orientation more complicated.

Let us consider the magnetisation of the ferromagnetic slurry in the magnetic field. As is known, a magnetisation vector or a magnetic moment of the volume unit of a substance is a quantitative criterion of its magnetisation.

$$\vec{I} = \frac{\Delta \vec{p}_m}{\Delta V}, \tag{18}$$

where $\Delta \vec{p}_m$ is the total magnetic moment of the volume $\Delta V$ of the magnet.

We denote the volume fraction of the solid component in the slurry by $W_\tau$. Let us select the volume $\Delta V$ in the magnetised slurry and determine its magnetisation as a module of the magnetisation vector.

$$|\vec{I}| \equiv I. \tag{19}$$

We denote the value of magnetisation of pure magnetite (100%) by $I_M$ and determine the magnetic moment of the volume $\Delta V$ of the slurry if it is within the magnetic field $H > H_n$ (magnetic field intensity under which saturation starts). We shall assume that the value $\eta$ determines the fraction of the magnetic component in the slurry solid phase. In this case, magnetisation will be determined by the following expression:

$$I_{sl} = \frac{W_\tau \ \eta \Delta V I_M}{\Delta V} = W_\tau \eta I_M. \tag{20}$$

On the other hand, it is known that magnetisation of a substance (including slurry) is determined by the magnetic field intensity $H$:

$$I_{sl} = \chi H, \tag{21}$$

where $\chi$ is the magnetic susceptibility of the substance.

Setting the left and the right parts of Eqs (20) and (21) equal, we obtain

$$\chi H = W_\tau \eta I_M. \tag{22}$$

When using Lamb waves to assess the volume fraction of the slurry solid phase, the following signal is formed (Morkun et al., 2014):

$$S \equiv ln\left(\frac{I_{0,v}}{I_{l,v}}\right) = W_\tau \frac{(\rho_{sol} - \rho_w)}{\rho} C. \tag{23}$$

After dividing the left and the right parts of Eqs (13) and (14), we obtain

$$\frac{\chi H}{ln\left(\frac{I_{0,v}}{I_{l,v}}\right)} = \frac{W_\tau \eta I_M}{W_\tau \frac{(\rho_{sol} - \rho_w)}{\rho} C_v} = \frac{\eta I_M}{\frac{(\rho_{sol} - \rho_w)}{\rho} C_v}. \tag{24}$$

It follows from Eq. (24) that

$$\eta = \left[\frac{(\rho_{sol} - \rho_w)}{\rho I_M} C\right] \frac{\chi H}{ln\left(\frac{I_{0,v}}{I_{l,v}}\right)}. \tag{25}$$

The expression in square brackets is almost a constant value denoted by $A$. Then, Eq. (25) will become shorter

$$\eta = A \frac{\chi H}{ln\left(\frac{I_{0,v}}{I_{l,v}}\right)} = A \frac{(\mu - 1) H}{ln\left(\frac{I_{0,v}}{I_{l,v}}\right)}, \tag{26}$$

where $\mu_r = 1 + \chi$ is the relative magnetic permeability of the slurry within the magnetic field of intensity $H$. This formula is the basis for determining the fraction of the magnetic component in the solid phase of the slurry.

## 6. DISCUSSION OF MATERIALS

The general scheme for measuring the ferromagnetic component in the iron ore slurry flow is given in Fig. 7.

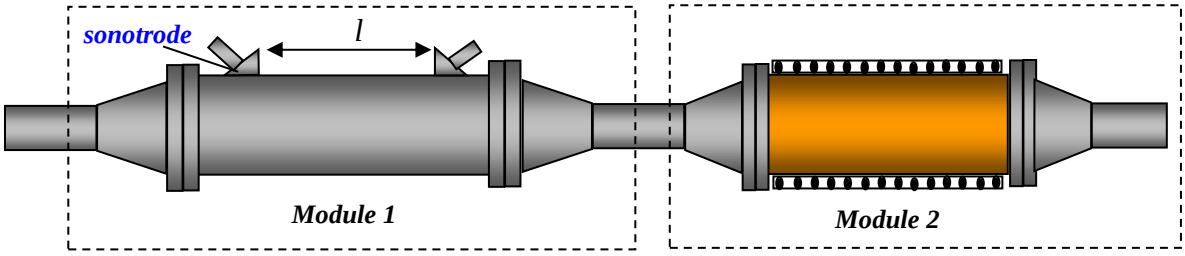


**Fig. 7.** Scheme for measuring the ferromagnetic component content in the slurry flow

In measuring Module 1, ultrasonic control of the volume fraction of the solid phase of the slurry is performed by means of Lamb waves (5 MHz), which extend from the sonotrode to a receiver, which are arranged at a distance $l$ = 300 mm. In measuring Module 2, the slurry is magnetised and its magnetic susceptibility is measured. Measuring Module 2 is a solenoid containing $n$ winds per unit length (Fig. 8). When direct current is imposed through the solenoid $J_0$, a homogeneous magnetic field of intensity $H$ appears inside it:

$$H = n \cdot J_0. \tag{27}$$

To determine magnetic susceptibility $\mu$, we apply the known ratio

$$H = \frac{B}{\mu \mu_0}, \tag{28}$$

where $B$ is the magnetic flux density in the slurry, and $\mu_0$ is the magnetic permeability of vacuum.

Thus, it is necessary to measure *B* and *H* to determine $\mu$. If *H* is definitely determined through conduction currents $J_o$ according to Eq. (27), in order to find *B*, we can use classical measuring schemes. Fig. 7 presents one of the ways of determining *B*. If the vessel walls of the measuring module are made of non-magnetic material, we can define the value *B* by means of the auxiliary winding *3* or coil *4*.

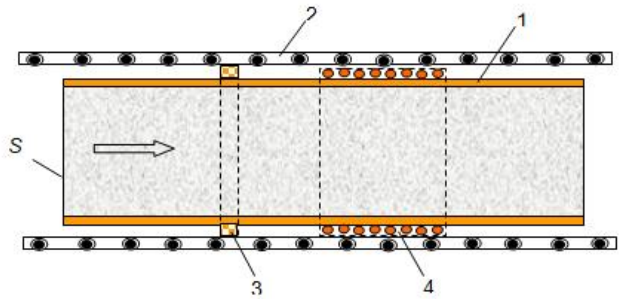


**Fig. 8.** Measuring Module 2 for determining the magnetic characteristics of the slurry: 1 - walls of the vessel with the slurry; 2 –solenoid winding; 3,4 – auxiliary winding or coil; S – cross-sectional area

While switching on and off the magnetic field, there appears a short-time current in the auxiliary coil and a charge *q* runs along the circuit, the value of which is proportional to the magnetic flux density *B*:

$$q = \frac{N \cdot S \cdot B}{R}, \tag{29}$$

where *N* is the number of winds of the auxiliary coil, *S* is the area of the cross-section determined by the inner diameter of the module, *R* is the full resistance of the measuring circuit (resistance of the winding of the auxiliary coil and input resistance of the measuring device).

Thus, by measuring the full charge of the short-time current in the auxiliary coil, we can determine *B:*

$$B = \frac{q \cdot R}{N \cdot S} \tag{30}$$

$$\mu = \frac{B}{\mu_o H} = \frac{qR}{\mu_o NSnJ_o} = qC_1. \tag{31}$$

where $C_1 = \frac{R}{\mu_0 NSnJ_0}$ is a constant value.

The final expression for finding the fraction of the magnetic component $\eta$ in the slurry looks as follows:

$$\eta = A\frac{(\mu-1)H}{ln\left(\frac{I_{0,v}}{I_{l,v}}\right)} = (AnJ_o)\frac{(qC_1-1)}{ln\left(\frac{I_{0,v}}{I_{l,v}}\right)} = A_1\frac{(qC_1-1)}{ln\left(\frac{I_{0,v}}{I_{l,v}}\right)}. \tag{32}$$

The constants $A_1$ and $C_1$ are determined by calibrating the system. The constant $C_1$ is determined in laboratory conditions in the way described below.

In the empty measuring Module 2, the charge $q_c$ is measured while switching on/off the magnetic field. If the value of $\mu_r$ for the air can be considered equal to '1', the following condition is observed:

$$q_c C_1 - 1 = 0. \tag{33}$$

This results in

$$C_1 = \frac{1}{q_c}. \tag{34}$$

The second calibration stage is conducted in the real slurry. Measurements are conducted in both modules, and the value $\frac{(qC_1-1)}{ln\left(\frac{I_{0,v}}{I_{l,v}}\right)}$ is determined. Then, the slurry is selected for analysing the magnetic component content $\eta$. The proportionality factor is found according to Eq. (32):

$$A_1 = \frac{\eta}{\left[\frac{(qC_1-1)}{ln\left(\frac{I_{0,v}}{I_{l,v}}\right)}\right]}. \tag{35}$$

If the measuring Module 2 is made of magnetic material, the auxiliary measuring coil should be placed inside it. A measuring probe placed inside the module can be another option (Fig. 9).

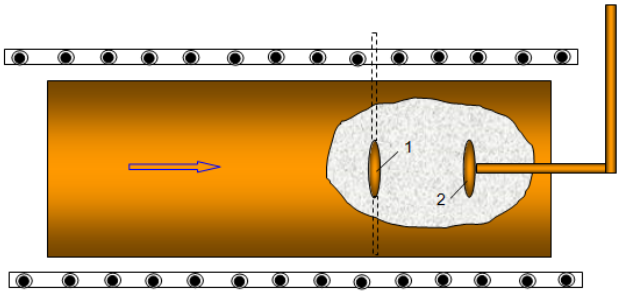


**Fig. 9.** Variant of measuring Module 2 for determining the magnetic characteristics of the slurry by means of inner probes

The probe should be a prolate ellipsoid to ensure homogeneity of the magnetic field inside the probe (Fig. 10). Besides, it should be made of non-magnetic material. The shape of the ellipsoid should create a narrow clearance corresponding to the washer. With this shape, the magnetic field *B* inside the probe is close to the field in the slurry.

There is either a circular coil or a Hall sensor inside the probe (Fig. 9). For the circular coil, the procedure of determining the magnetic component does not change and is relevant to the above. As for the Hall sensor, instead of measuring the charge, voltage is measured and determined by the following expression:

$$\Delta U = R_x jaB = C_x B. \tag{36}$$

where *j* is the current density; *a* is a design factor of the sensor; and $R_x$ is the Hall constant.

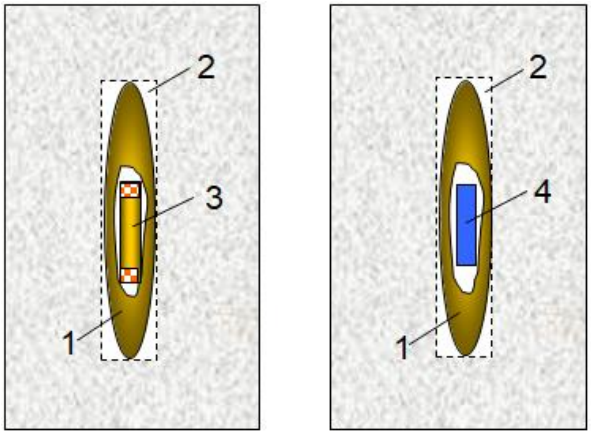


**Fig. 10.** Structure of the measuring probe: 1 – measuring probe; 2 – internal cavity equivalent to the probe; 3 –measuring coil; 4 – Hall sensor

It follows from the formula that the magnetic flux density $B$ is proportional to voltage $\Delta U$. So, the magnetic component $\eta$ in the slurry can be found according to the following expression.

$$\eta = A_2 \frac{(\Delta U C_2 - 1)}{ln\left(\frac{I_{0,\nu}}{I_{l,\nu}}\right)}, \quad (37)$$

which is similar to Eq. (32).

The results of testing the device used for controlling the content of the ferromagnetic component in the slurry flow are given in Fig. 11.

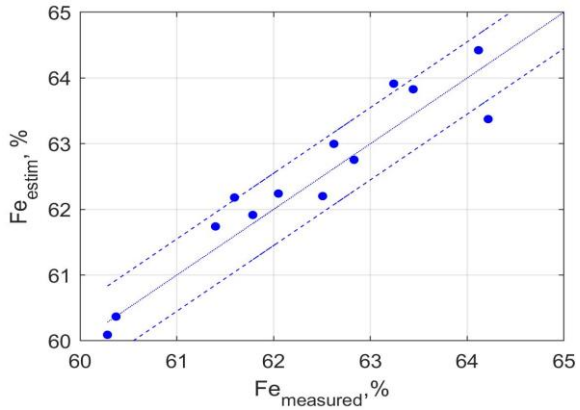


**Fig. 11.** Testing results of the device for controlling the ferromagnetic component content in the slurry flow

The results of testing of the device used for controlling the content of the ferromagnetic component in the slurry flow by ultrasonic and magnetic measurements indicate that the error in measurement of the iron content in the solid phase of the slurry does not exceed 0.47%.

## 7. CONCLUSIONS

The results of laboratory and industrial testing of the device developed for controlling the ferromagnetic component content in the slurry flow by ultrasonic and magnetic methods indicate its high accuracy and reliability. Considering the fact that the error of measuring iron content in the solid phase of the slurry does not exceed 0.47%, it can be recommended for wider application at magnetic concentration plants as a CAPCS means.

## REFERENCES

1. **Bogdanov, O.S.** (1983), *Ore dressing guide*. Nedra, Moscow. in Russian.
2. **Bond, L.J., Morra, M., Greenwood, M.S., Bamberger, J.A., Pappas, R.A.** (2003), Ultrasonic technologies for advanced process monitoring, measurement, and control, *Proceedings of the 20th IEEE Information and Measurement Technology Conference*, 2, 1288-1293.
3. **Brazhnikov, N.I.** (1975), *Ultrasonic methods*, Energia, Moscow. in Russian.
4. **Debarnot, M. Le Letty, R., Lhermet, N.** (2006), Ultrasonic NDT based on Lamb waves: Development of a dedicated drive and monitoring electronic, *Proceedings of the 3rd EuropeanWorkshop on Structural Health Monitoring*, 1207–1213.
5. **Derkach, V.G.** (1966), *Special Methods for Mineral Processing*. Nedra, Moscow. in Russian.
6. **Eremenko, Y., Poleshchenko, D., Tsygankov, Y.** (2019), Neural network based identification of ore processing units to develop model predictive control system, *Proceedings of XXI International Conference Complex Systems: Control and Modeling Problems (CSCMP)*, 121-124.
7. **Eskandari, M.J., Hasanzadeh, I.** (2021), Size-controlled synthesis of Fe3O4 magnetic nanoparticles via an alternating magnetic field and ultrasonic-assisted chemical co-precipitation, *Materials Science and Engineering B-advanced Functional Solid-State Materials*, 266, 115050.
8. **Fukumoto, T., Tanaka, Y., Sawada, T.** (2019), Change of ultrasonic propagation velocity in an MR fluid under AC magnetic fields, *International Journal of Applied Electromagnetics and Mechanics*, 1(59), 341-347.
9. **Golik, V., Komaschenko, V., Morkun, V., Khasheva, Z.** (2015a), The effectiveness of combining the stages of ore fields development, *Metallurgical and Mining Industry*, 7(5), 401-405.
10. **Golik, V., Komashchenko, V., Morkun, V.** (2015b), Geomechanical terms of use of the mill tailings for preparation, *Metallurgical and Mining Industry*, 7(4), 321-324.
11. **Hauptmann, P., Hoppe, N., Püttmer, A.** (2002), Application of ultrasonic sensors in the process industry, *Measurement Science and Technology*, 13 (8), R73-R83. DOI: 10.1088/0957-0233/13/8/201.
12. **Karmazin, V.I., Karmazin, V.V.** (1978), *Magnetic enrichment methods*, Nedra, Moscow. in Russian.
13. **Kupin, A.** (2014), Application of neurocontrol principles and classification optimization in conditions of sophisticated technological processes of beneficiation complexes, *Metallurgical and Mining Industry*, 6, 16–24.
14. **Lee, C., Staszewski, W. J.** (2009), Modelling of Lamb waves for damage detection in metallic structures: Part I. Wave propagation, Smart *Materials and Structures*, 12(5), 804.
15. **Liu, B.Y., Liu, B.J., Gao, X.W., Zhang, D.S., Hao, D.Z., Li, X.Y.** (2020), A soft sensor based on case-based reasoning for iron ores flotation, *Ironmaking & Steelmaking*, 2(47), 150-158.
16. **Lolaev, A.B., Meshkov, E.I., Kovalyova, M.A.** (2018), Research and development of automated system of solids flow control in the slurry entering the tailings storage facility along a pipeline with a varying degree of filling, *Sustainable Development of Mountain Territories*, 10(2), 253-259. DOI: 10.21177/1998-4502-2018-10-2-253-259.
17. **Louisnard, O.** (2012a), A simple model of ultrasound propagation in a cavitating liquid. Part I: Theory, nonlinear attenuation and traveling wave generation, *Ultrasonics Sonochemistry*, 19(1), 56–65.
18. **Louisnard, O.** (2012b), A simple model of ultrasound propagation in a cavitating liquid. Part II: Primary Bjerknes force and bubble structures, *Ultrasonics Sonochemistry*, 19(1), 66–76.
19. **Ma, L.C., Zhang, Y., Song, G.Q., Ma, Z., Lu, T.Q.** (2019), Ore granularity detection and analysis system based on image processing, *Proceedings of the 2019 31st Chinese Control and Decision Conference (CCDC 2019)*, 359-366.
20. **Meng, Y.Y., Yan, S.** (2019), Thin plate Lamb propagation rule and dispersion curve drawing based on wave theory, *Surface Review and Letters*, 7(26), 1850222.
21. **Modlo, Y.O., Semerikov, S.O., Bondarevskyi, S.L., Tolmachev, S.T., Markova, O.M., Nechypurenko, P.P.** (2019), Methods of using mobile Internet devices in the formation of the general scientific component of bachelor in electromechanics competency in modeling of technical objects, *Proceedings of the 2nd International Workshop on Augmented Reality in Education (AREDU 2019)*, 2547, 217-240.
22. **Morkun, V., Morkun, N., Pikilnyak, A.** (2014), The adaptive control for intensity of ultrasonic influence on iron ore pulp, *Metallurgical and Mining Industry*, 6(6), 8-11.
23. **Morkun, V., Morkun, N., Tron, V.** (2015a), Model synthesis of nonlinear nonstationary dynamical systems in concentrating production using Volterra kernel transformation, *Metallurgical and Mining Industry*, 7(10),6-9.

24. **Morkun, V., Morkun, N., Tron, V.** (2015b), Distributed control of ore beneficiation interrelated processes under parametric uncertainty, *Metallurgical and Mining Industry*, 7(8), 18-21.
25. **Morkun, V., Morkun, N., Tron, V.** (2015c). Distributed closed-loop control formation for technological line of iron ore raw materials beneficiation, *Metallurgical and Mining Industry*, 7(7), 16-19.
26. **Ni, L., Chen, X.** (2018), Mode separation for multimode Lamb waves based on dispersion compensation and fractional differential, *Acta Physica Sinica*, 20(67), 204301.
27. **Parekh, K., Patel, J., Upadhyay, R.V.** (2015), Ultrasonic propagation: A technique to reveal field induced structure in magnetic nanofluids, *Ultrasonics*, 60, 126-132.
28. **Parekh, K., Upadhyay, R.V.** (2017), The effect of magnetic field induced aggregates on ultrasound propagation in aqueous magnetic fluid, *Journal of Magnetism and Magnetic Materials*, 431, 74-78.
29. **Porkuian, O., Morkun, V., Morkun, N., Tron, V., Haponenko, I., Davidkovich, A.** (2020), Influence of the magnetic field on love waves propagation in the solid medium, *Proceedings of IEEE 40th International Conference on Electronics and Nanotechnology (ELNANO)*, 761-766.
30. **Ryden, N., Park, C.B., Ulriksen, P., Miller, R.D.** (2003), Lamb wave analysis for non-destructive testing of concrete plate structures, *Symposium on the Application of Geophysics to Engineering and Environmental Problems (SAGEEP 2003)*.
31. **Rzhevsky, V.V., Yamshchikov, V.S**. (1968), *Ultrasonic monitoring and research in mining*, Nedra, Moscow. in Russian.
32. **Seip, R., VanBaren, P., Cain, C., Ebbini, E.** (1996), Noninvasive real-time multipoint temperature control for ultrasound phased array treatments, *IEEE Transactions on Ultrasonics, Ferroelectrics, and Frequency Control*, 6, 1063–1073.
33. **Semerikov, S., Slovak, K.** (2011), Theory and methodics of mobile mathematical tools using in the process of higher mathematics teaching for students of economic specialties, *Information Technologies and Learning Tools*, 1(21).
34. **Stupnik, M.I., Kalinichenko, V.O., Kalinichenko, O.V., Muzyka, I.O., Fedko, M.B., Pysmennyi, S.V.** (2015), Information technologies as a component of monitoring and control of stress-deformed state of rock mass, *Mining of Mineral Deposits*, 2(9), 175-181.
35. **Subhash, N., Krishnan, B.** (2011), Modelling and experiments for the development of a guided wave liquid level, *Proceedings of the National Seminar & Exhibition on Non-Destructive Evaluation*, 240–244.
36. **Viktorov, I.A.** (1966), *Physical fundamentals of the application of Rayleigh and Lamb ultrasonic waves in technology*, Nauka, Moscow. in Russian.
37. **Viktorov, I.A.** (1975), Elastic waves in a solid half-space with a magnetic field, *Reports of the USSR Academy of Sciences*, 221(5), 1069–1072. in Russian.
38. **Wan, Z.P., He, Z.C., Wang, X.W., Chen, B.Q., Ong, R.H., Zhao, Y.L.** (2020), Heat transfer in a liquid under focused ultrasonic field, *Experimental Thermal and Fluid Science*, 119, 110179.
39. **Weinberg, A.K.** (1966), Magnetic permeability, electrical conductivity, dielectric constant and thermal conductivity of a medium containing spherical and ellipsoidal inclusions, *Reports of the USSR Academy of Sciences*, 169(3), 543-546. in Russian.
40. **Xu, Y.F., Hu, W.X.** (2017), Wideband dispersion removal and mode separation of Lamb waves based on two-component laser interferometer measurement, *Chinese Physics B*, 9(26), 094301.
41. **Yuan, Y., Miao, B.Y., An, Y.** (2018), Cavitation clouds in gas-containing liquids block low-frequency components of ultrasonic waves, *Journal of Applied Physics*, 22(124), 224902.
42. **Zhang, Y.H, Qian, Z.H., Wang, B.** (2020), Modes control of Lamb wave in plates using meander-line electromagnetic acoustic transducers, *Applied Sciences-Basel*, 10(10), 3491.
43. **Zhao, S.N., Yao, C.Q., Zhang, Q., Chen, G.W., Yuan, Q.** (2019), Acoustic cavitation and ultrasound-assisted nitration process in ultrasonic microreactors: The effects of channel dimension, solvent properties and temperature, *Chemical Engineering Journal*, 374, 68-78.

Vladimir Morkun: https://orcid.org/0000-0003-1506-9759
Natalia Morkun: https://orcid.org/0000-0002-1261-1170
Vitaliy Tron: https://orcid.org/0000-0002-6149-5794
Olga Porkuian: https://orcid.org/0000-0003-3595-8211
Oleksandra Serdiuk: https://orcid.org/0000-0003-1244-7689
Tetiana Sulyma: https://orcid.org/0000-0002-8869-040X